Open Archive TOULOUSE Archive Ouverte (OATAO)
OATAO is an open access repository that collects the work of Toulouse researchers and makes it freely available over the web where possible.

This is an author-deposited version published in : http://oatao.univ-toulouse.fr/
Eprints ID : 14217

To link to this article : doi: 10.1002/pssc.201510037
URL : http://dx.doi.org/10.1002/pssc.201510037

To cite this version : Etchepare, Pierre-Luc and Baggetto, Loïc and Vergnes, Hugues and Samélor, Diane and Sadowski, Daniel and Caussat, Brigitte and Vahlas, Constantin Process-structure-properties relationship in direct liquid injection chemical vapor deposition of amorphous alumina from aluminum tri-isopropoxide. (2015) physica status solidi (c), vol. 12 (n° 7). pp. 944-952. ISSN 1862-6351

Any correspondance concerning this service should be sent to the repository administrator: staff-oatao@listes-diff.inp-toulouse.fr

DOI 10.1002/pssc.201510037

Process-structure-properties relationship in direct liquid injection chemical vapor deposition of amorphous alumina from aluminum tri-isopropoxide

Pierre-Luc Etchepare[*,1], Loïc Baggetto[1], Hugues Vergnes[2], Diane Samélor[1], Daniel Sadowski[1], Brigitte Caussat[2], and Constantin Vahlas[*,1]

[1] Centre Interuniversitaire de Recherche et d'Ingénierie des Matériaux, ENSIACET/INPT, Université de Toulouse, France
[2] Laboratoire de Génie Chimique, ENSIACET/INPT, Université de Toulouse, France

Keywords aluminum isopropoxide, amorphous alumina films, direct liquid injection, hydrothermal ageing, glass surface

[*] Corresponding authors: e-mail pierreluc.etchepare@ensiacet.fr; constantin.vahlas@ensiacet.fr

We propose a method to apply amorphous alumina films on the inner surface of glass containers aiming to improve their hydrothermal barrier property. We have carried out alumina deposition on Si substrates as a function of deposition temperature to determine the physico-chemical properties of the thin film materials, and on glass containers to evaluate the influence of post-deposition hydrothermal ageing on the films properties. Film preparation has been achieved by metal-organic chemical vapor deposition (MOCVD), using tri-isopropoxide aluminum (ATI) dissolved in anhydrous cyclohexane as precursor, in a temperature range between 360 °C and 600 °C. A direct liquid injection technology is used to feed the reactor in a controlled and reproducible way. The amorphous alumina films have been characterized by several techniques such as XRD, EPMA, XPS, SEM, AFM and scratch-test method. Films are amorphous and hydroxylated at 360 and 420 °C and close to stoichiometric at 490 and 560 °C. Hydrothermal ageing simulated by a standard sterilization cycle modifies the adhesion and surface morphology of the alumina film on glass containers to a rough, porous and non-adhesive layer.

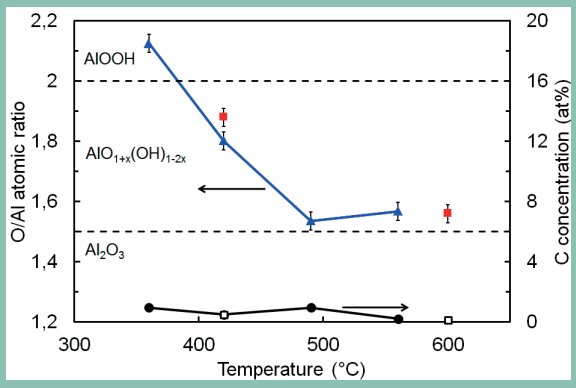

Elemental compositions of alumina films on Si substrates. O/Al atomic ratios (EPMA) for films processed in the horizontal (blue dots) and vertical (red dots) reactors. Carbon concentration for films deposited in the horizontal (black dots) and vertical (white dots) reactors, determined, respectively, by XPS and EPMA. Films processed at high temperatures (490-560 °C) are stoichiometric Al_2O_3 with a very low amount of hydroxyl groups. Carbon concentrations are lower than 1 at%.

1 Introduction Due to their numerous allotropic phases and their tunable crystallinity, alumina films are materials of major technological and industrial potential. Their various properties match a wide panel of applications such as optical transmittance for optics [1], insulating properties for microelectronic components [2], wear resistance [3], catalyst support [4], protection against corrosion [5] and barrier properties [6]. Specifications often require a dense, robust and adherent coating for protecting metal, glass or polymer surfaces with specific properties. In particular, amorphous alumina films present interesting physico-chemical characteristics whose nature, extent and combination depend on the preparation conditions [7, 8].

Different techniques have been applied to process alumina coatings on metal or polymer substrates such as electron beam evaporation [9], rf magnetron sputtering [2], atomic layer deposition [10, 11], sol-gel [5] or metalorganic CVD (MOCVD) [7, 12-14]. The latter is one of the most attractive techniques for the deposition of such films on complex-in-shape geometries with conformal coverage i.e. uniform thickness along the surface. Composition, allotropic phases, stoichiometry, crystallinity and microstructure of the material can be adjusted by fine tuning of the MOCVD experimental parameters such as reactor design, precursor selection, reactive atmosphere, deposition temperature and pressure. The MOCVD of alumina from aluminum tri-isopropoxide (ATI) is well documented [7, 8, 12-19]. ATI yields amorphous and stoichiometric alumina coatings with a smooth and dense microstructure at 5 Torr in the temperature range 420 °C to 650 °C [8, 15, 19]. Higher process temperatures lead to the deposition of nano-crystallized γ-Al_2O_3 [15] or to the homogeneous decomposition of ATI which generates a different microstructure [12]. The ATI molecule is well described in the literature [20]. It is sensitive to water vapor and thus it is subjected to ageing upon exposure to ambient atmosphere, which results in its partial or total hydrolysis in non-volatile compounds, $Al(O^iPr)_{3-n}(OH)_n$ (n=1, 2) and $Al(OH)_3$ respectively [13, 20]. The precursor is usually melted, maintained in supercooled state and vaporized with a bubbler. Despite the simplicity and the cost effectiveness of this solution, the use of ATI in the supercooled state has two consequences. First, maintaining ATI at the vaporization temperature for a long period impacts the stability of the molecule and subsequently the coating quality [13]. Second, it is difficult to know exactly the generated reactive gas mass flow rate. This poorly controlled situation leads to non-reproducible processes, especially for the present case where low activation energy prevails in the entire temperature range of interest, *de facto* resulting in mass transport limited process. The direct liquid injection (DLI) technology allows overcoming the previously mentioned drawbacks with the controlled atomization and vaporization of ATI dissolved in a carrier solvent [21, 22]. The DLI of ATI is not well documented in the literature except by Song et al. [23] and Krumdieck et al. [14] who implemented it in a pulsed-pressure MOCVD process. The authors used a solution of ATI in n-octane and in dry toluene, respectively. Films obtained between 500 and 550 °C at a nominal base pressure of 0.6 Torr were stoichiometric, amorphous and presented a nodular surface morphology.

We recently investigated a DLI-MOCVD process for the application of amorphous alumina from ATI on the internal surface of glass bottles with the aim to increase their barrier properties. We reported on the process modeling involving the development of a numerical model, using the Computational Fluid Dynamics code FLUENT, to calculate local profiles of gas flow, temperature, concentration and deposition rates inside the bottle. Interplay between simulation and deposition experiments allowed identifying process conditions which led to the deposition of transparent films with uniform thickness profile [24, 25].

In the present work we report on the experimental investigation of the process-structure-properties relationship of this film. First, we focus on the dissolution of ATI, with the aim to establish criteria for the selection of the different solvents and define the most appropriate one. Then, we detail results on the deposition of alumina films on silicon wafers and glass containers. We are especially interested on the possible impact of the solvent on the films composition and characteristics. Finally, we report on the hydrothermal ageing of the alumina coated glass substrates using a standard sterilization cycle in terms of surface morphology and adhesion, before providing concluding remarks.

2 Materials and methods

2.1 Thin film preparation The precursor solution was prepared by mixing ATI and anhydrous cyclohexane inside a Schlenk flask. The viscosity of 0.05 M to 1 M solutions of ATI in cyclohexane was measured with a falling sphere viscometer. The turbidity, i.e. the presence of insoluble particles in the solvent was measured for highly concentrated solutions in cyclohexane and n-octane by the nephelometry method employing a Hach 2100 instrument. ATI powder (98%, Acros Organics) was weighed and sealed in a Schlenk flask inside a glovebox circulated with purified Ar (99.9997%, Air Products). The sealed flask was filled outside of the glovebox with the appropriate quantity of anhydrous cyclohexane (99.5%, H_2O < 10 ppm, Acros Organics) using an air-tight, Ar-purged, glass syringe to prepare a solution of varying concentration from 0.025 to 1 M. Then, the Schlenk flask was connected with the injection system and purged several times with pressurized N_2 (99.9999%, Praxair). DLI of the solution was carried out with Kemstream Vapbox® systems. One gas line was connected to the injection system consisting of a N_2-pressurized Schlenk flask filled with the precursor solution and connected to a set of two injectors. During the deposition, the ATI solution was injected through an injector to form small droplets with a calculated flow rate from 0.90 to 1.55 mL min^{-1}. The frequency (2 or 3 Hz) and opening times (from 3 to 30 ms) of the injection system were controlled by a computer interface. The injected solution was blended in the mixing chamber with carrier gas (pure N_2) with a pressure differential held at 1 bar. The mixing carrier gas flow of N_2 was fixed to a flow rate of 300 standard cubic centimeters per minute (sccm).

Glass containers (42.5 mm diameter, 73 mm height bottles) and Si substrates (10x10 mm, cut from 4" Si (100) wafers (Sil'tronix)) were cleaned in an ultrasonic bath with acetone and ethanol. DLI-MOCVD was performed in two different reactors.

Deposition onto Si substrates was carried out using a horizontal hot-wall reactor composed of a quartz tube (25 mm diameter, 300 mm length) heated by a resistive fur-

nace. Samples were placed on a stainless steel (SS) holder in the center of the quartz tube where the temperature was uniform. The total flow rate of the carrier gas with vaporized solution was maintained unchanged at 814 sccm. The inlet ATI molar fraction was estimated to be 8.2×10^{-3}.

Deposition on the inner walls of glass containers was performed in a vertical hot-wall DLI-MOCVD reactor, as described in detail elsewhere [24]. It is recalled that the reactive gas phase was driven with pure N_2 and introduced through a SS nozzle from the upper part of the quartz tube. In this configuration, the total flow rate and the inlet ATI molar fraction were equal to 585 sccm and 1.7×10^{-3}, respectively. A SS holder maintained the glass container in the gas feeding tube axis. An inductively heated thermoregulated SS cylinder around the reaction chamber ensured a temperature profile along the container with a set temperature at the bottom external surface on the central axis of the container 480 °C [23].

In both systems, the vaporization chamber and SS transport lines were thermally regulated to allow efficient flash vaporization of the mixture droplets without early ATI decomposition or partial solvent vaporization. Dry pumps (base pressure < 5.10^{-2} Torr) and pressure gauges connected to the output of the deposition chambers were used to control the reaction pressure to 5 Torr.

Coated glass containers were submitted to one sterilization cycle in wet atmosphere. Samples were filled with ultra-pure water (18.2 MΩ.cm) and placed during 1 h inside an autoclave (Getinge) operating at 121 °C and 2 bar absolute pressure. Heating and cooling rates were controlled to avoid thermal cracks.

2.2 Materials characterization X-ray diffraction (XRD) was performed on a Bruker D8 Advance using a Cu K_α (1.5418 Å) X-ray tube operated at 40 kV and 40 mA, a Ni filter and solid-state Lynxeye detector in θ-3°/θ+3° configuration. Samples were measured on a zero background holder and a θ offset of 3° was applied between the X-ray source and detector arms to suppress the strong diffraction of the Si substrates.

X-ray photoelectron spectroscopy (XPS) was performed on a Thermo Scientific K-Alpha instrument capable of a typical base pressure of 10^{-9} Torr using monochromatic Al K_α (1486.6 eV). The spectrometer energy calibration was performed using the Au4f7/2 (83.9 ± 0.1 eV) and Cu2p3/2 (932.7 ± 0.1 eV) photoelectron lines. Charging compensation and neutralization were applied by using a dual beam flood gun. The probed areas were about 400 µm diameter. Surface erosion was employed using Ar ions accelerated at 2 kV, resulting in an erosion rate of about 0.08 nm s^{-1}. Constant pass energy of 30 eV and energy steps of 0.1 eV were used for high resolution scans. The photoelectron peaks were analyzed by Gaussian/Lorentzian (G/L = 70/30) peak fitting and using a Shirley background. The atomic concentrations were determined from photoelectron peak areas using the atomic sensitivity factors reported by Scofield, taking into account the transmission function of the analyzer calculated at different pass energies from Ag3d and AgMNN peaks collected for a reference sample.

The O/Al ratios in the films were determined by electron probe microanalysis (EPMA) with a Cameca SXFive apparatus operated at 10 and 15 keV and calibrated using a high purity alumina standard. Samples were covered by a thin layer of carbon in a vaporization chamber (Leica) to prevent charging effects. Each sample was measured 12 times in different locations to determine the spatial homogeneity of the sample composition.

Scanning electron microscopy (SEM) on coated glass container fragments was performed with a LEO 435VP instrument. Samples were fractured and metalized with silver and graphite before analysis in order to avoid charging effects. Acquisition was performed with an acceleration voltage of 10 kV, a probe current between 40-80 pA and a working distance 11 mm. SEM on alumina films deposited on Si substrates was performed with a JEOL JSM-7800F field emission scanning electron microscope operated at 10 kV in backscattered mode. Samples were fractured and metalized with platinum before imaging.

The roughness of the alumina thin films deposited on the glass surface, before and after sterilization cycle was measured by atomic force microscopy (AFM) in tapping mode using an Agilent 5500 instrument. The probe silicon tip (AppNano ACT-50) with a spring constant of 13-77 N m^{-1} and resonance frequency between 200 and 40 kHz scanned areas of samples with a scan rate of 2 µm s^{-1} with 256x256 data points. Pico Image software (Agilent Technology) was used to analyze and process the data.

The adhesion of alumina coatings on glass containers before and after sterilization cycle was investigated by scratch-test method (standard EN 1071) using a CSM Revetest Instruments. Samples were scratched using a diamond indenter with a spherical tip of 200 µm and a cone angle of 120° at a constant loading rate of 15 N min^{-1}. The load applied on the coating surface increased from 1 to 30 N. The scratch track was fixed at 4 mm.

3 Results and discussion

3.1 Solubility of ATI The DLI technology requires dissolving the precursor in an appropriate solvent to inject and transport it to the deposition area. The selection of the solvent is an important step of the process optimization. It must take into account the physicochemical, and health and safety characteristics of the solvents, their cost, their compatibility with the precursor and their stability in the deposition conditions [26].

The solvent must have the same molecular dipole moments as the precursor to ensure maximum dissolution. The dipole moment of the ATI molecule equals 0 debye. For this reason the apolar solvents n-pentane, cyclohexane, n-heptane and n-octane were *a priori* considered since they also meet health and safety criteria excluding carcinogenic,

mutagenic and reprotoxic (CMR) substances. A tradeoff was applied for the final selection of the most appropriate solvent, based on four criteria: (a) The occupational exposure limit value (OELV) at 8 h which is also related to health and security but it depends on the countries legislation. (b) The boiling point which should be high enough to avoid partial vaporization of the solvent at ambient temperature in the Schlenk flask. (c) The saturated vapor pressure at the vaporization temperature (160 °C) which should be close enough to that of the precursor so as to prevent early vaporization of the solvent. (d) The ratio of the cost between each alkane and the less expensive solvent (cyclohexane) for ≥ 99% anhydrous quality. These criteria were rated in terms of importance as secondary, important and preponderant and then were weighed by a factor of 3, 5 and 8, respectively. This classification favors the preponderant criterion. Table 1 summarizes the data for each solvent. As for the four criteria, a coefficient of merit was attributed to each value ranging from 1 to 5 for the weaker to the stronger one.

Table 1 Weighed criteria and biological and physicochemical data for four apolar solvents. Each value is given a score of merit in parenthesis. The resulting total score for each solvent (last column) is the sum of the products of each weighed criterion times the score of merit. It appears that cyclohexane is the most appropriate solvent to dissolve and transport the ATI.

Criteria	OELV-8 h [ppm]	b.p. [°C]	$\frac{\log(P_{v.s.solv.})}{\log(P_{v.s.ATI})}$ at 160 °C	$\frac{\text{Cost(solv.)}}{\text{Cost}(C_6H_{12})}$	Total
Crit. weight	3	5	5	8	-
n-C_5H_{12}	1000 (5)	36 (1)	3.35 (1)	1.5 (3)	49
C_6H_{12}	200 (2)	81 (2)	2.98 (3)	1 (5)	71
n-C_7H_{16}	500 (3)	98 (2)	2.85 (3)	1.2 (4)	66
n-C_8H_{18}	300 (2)	126 (3)	2.63 (3)	5.1 (1)	44

N-pentane presents a low boiling point (36.1 °C) and a high saturated vapor pressure at 160 °C (ratio of 3.35 with ATI); i.e. an important risk of early vaporization. The saturated vapor pressure at 160 °C of n-heptane is high in comparison with that of ATI (ratio of 2.98) and its cost is relatively high. N-octane and cyclohexane present OELV and saturated vapor pressure close to some extent. Preliminary conclusions from this *a priori* investigation reveal that cyclohexane can be selected to dissolve and transport the ATI. However, additional criteria, such as viscosity and turbidity, dealing with the solubility of ATI *per se* should be considered to validate the selection of the cyclohexane.

The histogram of Fig. 1 shows the viscosity of the four solvents and of the corresponding solutions of ATI at 0.05 M fixed concentration, which is typical for an injected solution in a DLI-MOCVD process. The viscosity of the four solvents is low, not exceeding that of water (1 mPa s at 20 °C). Viscosities of the solutions are almost equal to those of pure solvents; they are compatible with DLI technology and are too close to each other to allow discrimination.

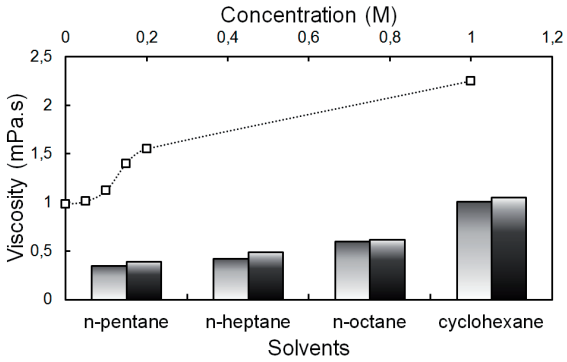

Figure 1 Viscosity of ATI solutions with n-pentane, n-heptane, n-octane and cyclohexane at 0.05 M fixed concentration (histogram, pure solvents and solutions in light and dark grey, respectively) and evolution of the viscosity of ATI solutions with cyclohexane as a function of concentration.

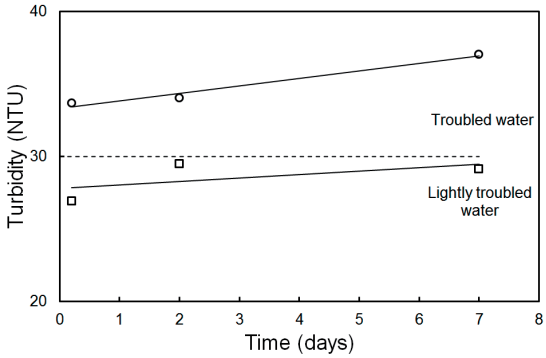

Figure 2 Turbidity values of 1M ATI solutions with cyclohexane (squares) and n-octane (circles). Limit value between lightly troubled water and troubled water at 30 NTU is indicated.

Figure 2 shows the evolution of the turbidity of 1 M solutions of ATI in cyclohexane and n-octane for comparison as a function of their ageing up to 7 days. It is worth noting that 1 M concentration and 7 days ageing are relatively high values for a CVD process. The turbidity of both solutions increases with ageing. That of the solutions with cyclohexane is systematically lower revealing a higher stability than the one with n-octane. Finally, the evolution of the viscosity of the ATI/cyclohexane solution as a function of concentration up to 1 M is shown in Fig. 1. The viscosity

increases from 0.98 mPa s at 0.05 M up to 2.25 mPa s at 1 M, i.e. to a value which is still convenient for DLI. A global consideration of these results reveals that cyclohexane is the most appropriate solvent for ATI. However, the solvent must not be subjected to thermal or reactive decomposition during deposition resulting in the pollution of the film. This criterion requires dedicated experimental investigation not detailed in the present article.

3.2 Film characteristics XRD patterns of films deposited on Si do not show any peaks associated with the formation of a crystalline structure for all deposition temperatures (see Fig. S1 of the Supporting Information, online at: www.pss-c.com).

Figure 3 shows the evolution of the O/Al atomic ratio and carbon concentration in the films deposited on Si, as a function of deposition temperature, determined by EPMA and XPS, respectively. The films grown onto Si substrates inside the horizontal CVD reactor (blue data points) prepared at 360 °C and 420 °C show O/Al atomic ratios equal to 2.12 and 1.80, respectively. These values correspond to compositions close to AlOOH (atomic ratio 2.0) and partially hydroxylated $AlO_{1+x}(OH)_{1-2x}$ films. Films prepared at 490 °C and 560 °C show O/Al ratios equal to 1.53 and 1.57, respectively, in good agreement with the formula Al_2O_3 (atomic ratio 1.5). Films deposited in the vertical CVD reactor (red data points) present O/Al ratios of 1.88 and 1.56 at 420 °C and 600 °C, respectively, in close agreement with those measured for the films grown in the horizontal CVD reactor. Hence, it appears that the inlet ATI molar fraction and the reactor configuration used here have little influence on the film composition.

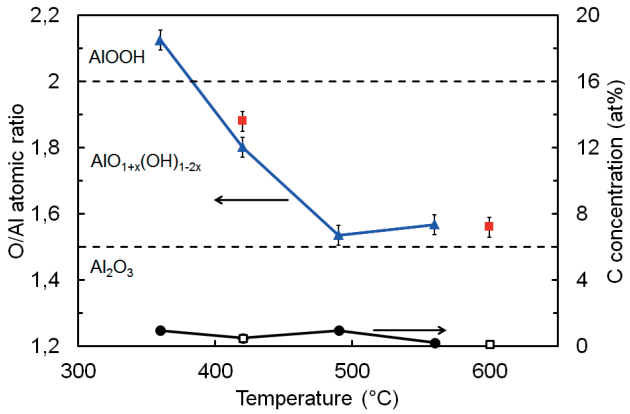

Figure 3 Elemental compositions of alumina films on Si substrates. O/Al atomic ratios were measured using EPMA for films processed in the horizontal (blue dots) and vertical (red dots) reactors. Carbon concentration was determined by XPS for films deposited in the horizontal reactor (black dots) and EPMA for those prepared in the vertical reactor (white dots).

The C content (black datapoints) measured by XPS after surface erosion is below 1 at% for all temperatures, similar to the C content measured by EPMA on films grown in the vertical reactor (black datapoints). Gleizes et al. measured similar O/Al atomic ratio (EPMA) for alumina films deposited by MOCVD with sublimed ATI in the temperature range of 480-600 °C [15].

The evolution of the elemental composition with deposition temperature observed by EPMA was further investigated using XPS. Films deposited on Si substrates were eroded by *ca.* 100 nm and subsequently measured with XPS (Fig. 4). The amount of aliphatic carbon (C-C and C-H bonds only) is less than 1 at% and likely results from small amounts of solvent residue incorporated in the film during growth.

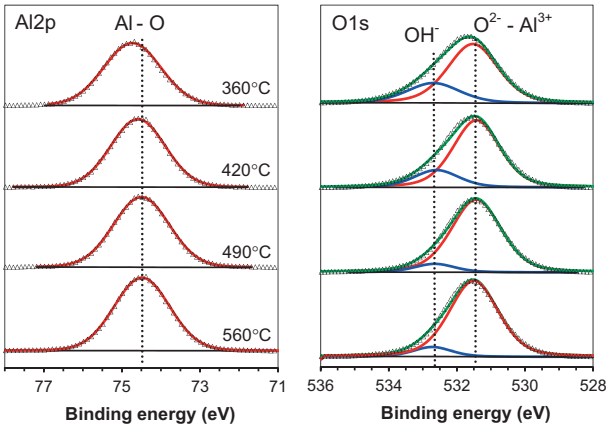

Figure 4 High resolution XPS spectra (Al2p and O1s) of alumina films deposited on Si substrates at 360 °C, 420 °C, 490 °C, and 560 °C. The decomposition of the spectra into the assigned chemical species is shown for each core level.

The Al2p signal apparently shows a single symmetric peak corresponding to Al^{3+} in an O^{2-} framework. The signals for Al2p in Al_2O_3, AlOOH and $Al(OH)_3$ are very close in binding energy and are consequently hard to separate [27-29]. The O1s signal is a better discriminant for the presence of hydroxyl groups, which have a peak expected at *ca.* 1.3 eV off the main O^{2-} peak of Al_2O_3 [27-29]. The measured O1s signals clearly show a main peak around 531.4 eV at the location expected for O^{2-} in the Al_2O_3 framework [30, 31], which is accompanied with a shoulder around 532.7 eV of increasing intensity with decreasing temperature, attributable to hydroxyl groups. The relative amount of hydroxyl groups increases with decreasing temperature, in agreement with the increasing O/Al ratio measured with EPMA. However the intensity of the response related to hydroxyls groups is not as intense as expected for a composition close to AlOOH obtained at 360 °C. This discrepancy likely results from ion beam damages, which decreases the actual quantity of OH signal. Nonetheless, the resulting spectra show a reasonable trend with the EPMA data. This is confirmed for instance in the case of the films deposited at 490 and 560 °C which show the presence of OH groups.

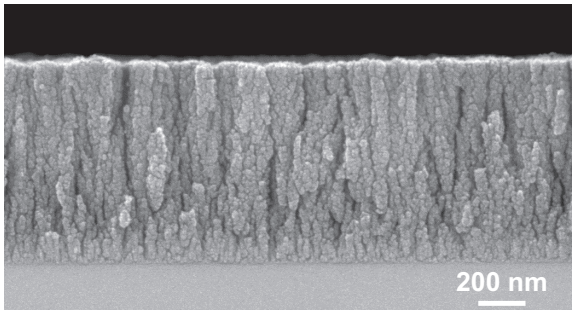

Figure 5 Cross-section SEM micrograph of amorphous alumina film on Si substrate for a deposition temperature of 480 °C.

The film morphology is shown in the cross-section SEM micrograph in Fig. 5. The film is smooth but slightly porous with nanometer cavities (see Fig. S2 of the Supporting Information) over the entire height, in contrast with alumina films deposited from sublimed ATI are very smooth and dense (see Fig. S2, [32]). This particular morphology may be attributed to the presence of cyclohexane in the DLI process.

3.3 Properties of films grown on the inner walls of glass containers The evolution of the surface morphology and adhesion of the film on glass substrates in wet atmosphere after a sterilization cycle was investigated. SEM micrographs of alumina films on glass container surfaces, before and after sterilization cycle, are presented in Fig. 6. The as-deposited film looks slightly rougher than the alumina films deposited on Si substrate in the horizontal reactor (Fig. 5). The higher roughness might be attributed to the glass surface topography. After a sterilization cycle, the film surface is significantly rougher and porous with sub-micrometric cavities.

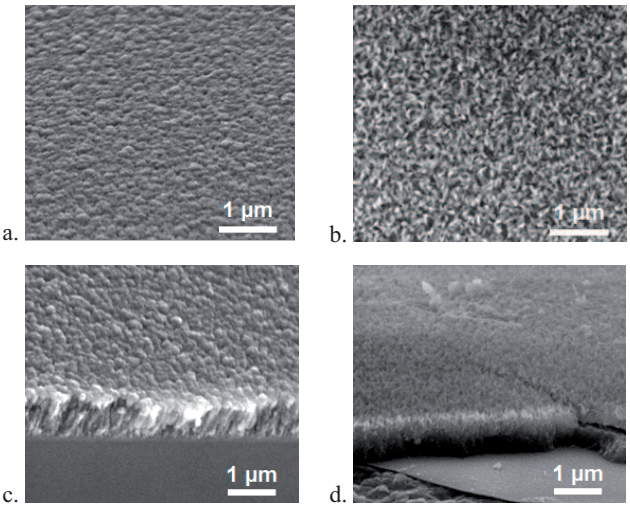

Figure 6 Surface (top) and cross-section (bottom) SEM micrographs of amorphous alumina deposited at 480 °C on glass containers before (a and c) and after a sterilization cycle (b and d). The flat part seen in part (d) is a bit of the glass bottle.

Surface 3D topography AFM images of alumina films deposited on glass containers before and after a sterilization cycle are shown in Fig. 7. Results of measured roughness for uncoated and coated containers are summarized in Table 2.

Table 2 Measured roughness of uncoated and coated containers before and after a sterilization cycle during 1 h at 121 °C.

	Uncoated containers		Coated containers	
	As processed	Sterilized	As processed	Sterilized
Roughness RMS (nm)	0.3	0.7	17.1	61.7

The root means square average of the roughness (RMS) of the bare containers is low (0.3 and 0.7 nm); i.e. the glass surface prior to deposition is extremely flat and smooth despite a slight increase of the surface roughness after the sterilization cycle. Before the sterilization cycle, alumina films display slightly rough features with a mean RMS value 17.1 nm. The sterilization cycle yields a strong increase of the roughness value to 61.7 nm which demonstrates the increase of surface porosity and subsequent film deterioration. From the SEM and AFM observations it is concluded that the ageing in such wet environment and relatively high temperature damages the film surface making it more porous and rougher.

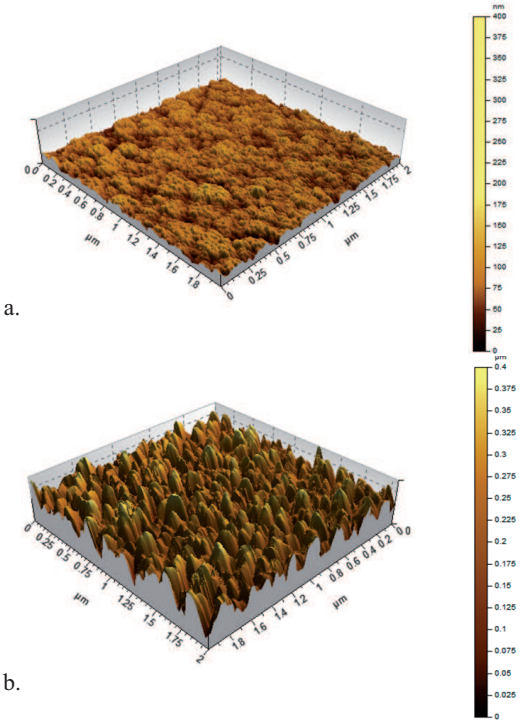

Figure 7 3D topography images of the surfaces measured by AFM employing the tapping mode for amorphous alumina films on the inner walls of glass containers before (a) and after a sterilization cycle (b).

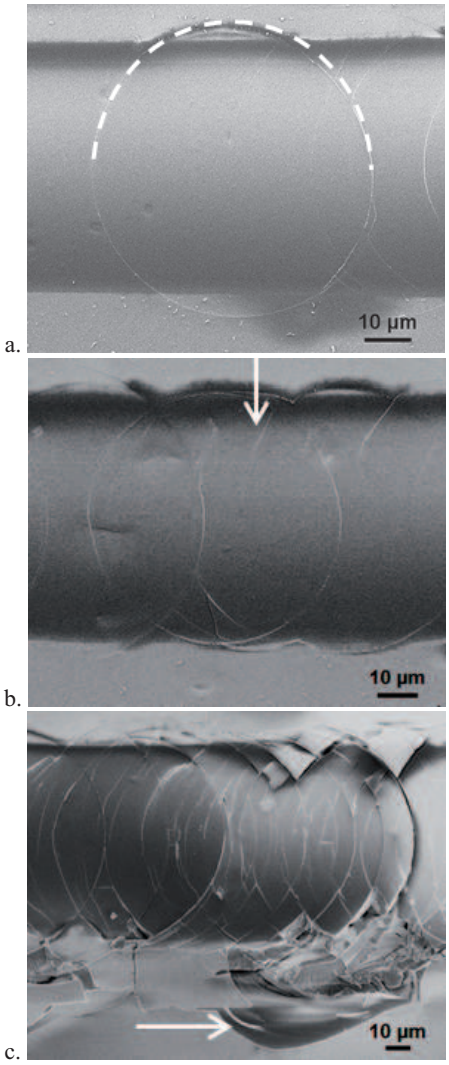

Figure 8 SEM micrographs of scratch tracks on the surface of alumina film deposited on glass containers at 480 °C before a sterilization cycle. Cracking failure modes depend on the indenter load and are defined as first cracks mode (a), lateral cracks mode (b), chipping mode (c). Dotted semicircle line and arrows are guide to the eye.

The effect of a sterilization cycle on the adhesion of the film on glass was investigated by scratch-test. SEM images of the tracks are presented in Fig. 8 before (Figs. 8a, b and c) and after (Figs. 9a, b, c and d) sterilization. These micrographs allow defining the features of four different coating failure modes. The first cracking mode (Figs. 8a and 9b) is determined by the presence of the indenter mark; i.e. the first circular crack on the film surface. The feature of the second cracking mode (Figs. 8b and 9c) is the propagation of lateral cracks perpendicular to the direction of scratch. The third mode (Figs. 8c and 9d) occurs with the coating chipping and the substrate exposure.

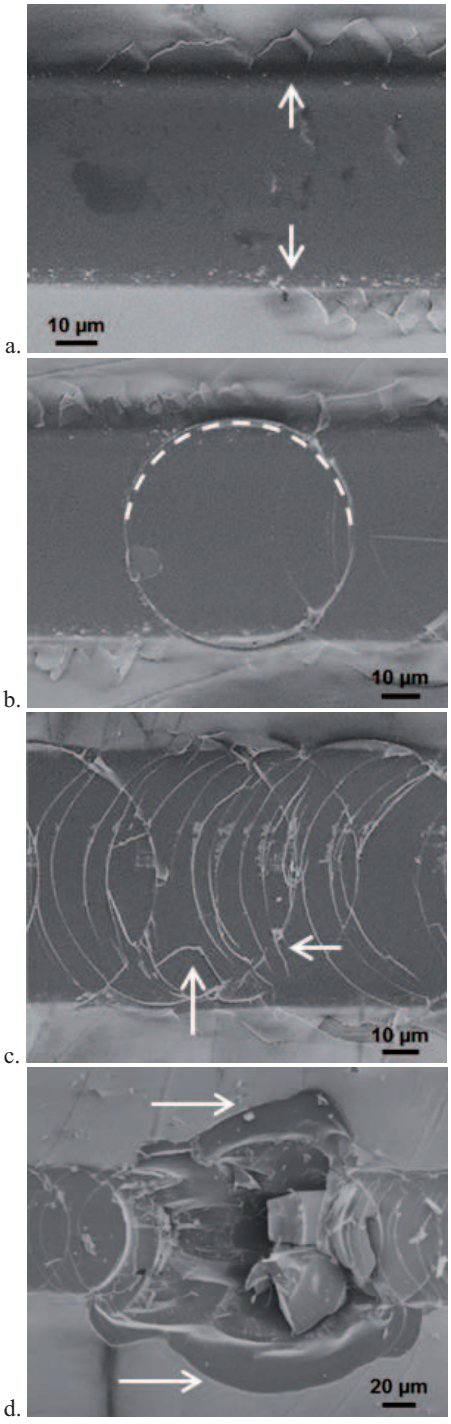

Figure 9 SEM micrographs of scratch tracks on the surface of alumina film deposited on glass containers at 480 °C after a sterilization cycle. Cracking failure modes depend on the indenter load and are defined as buckling/recovery spallation mode (a), first cracks mode (b), lateral cracks mode (c), chipping mode (d). Dotted semicircle line and arrows are guide to the eye.

An X-ray dispersive energy spectrometry analysis confirms the presence of an uncoated surface on the edges of the track; thus the total film delamination. The critical

loads were measured at the beginning of each cracking failure mode and are given in Table 3. All failure modes can be defined as Hertzian cracking [33] which corresponds to a through-thickness cracking of a hard coating (compressive stresses generated ahead of the indenter and tensile stresses behind it). Tensile cracking failure mode is also found in the literature for alumina coatings deposited on glass substrate [34]. An additional mode (Fig. 9a) is observed for sterilized coated containers with partial delamination only on the edges of the track at low loads. It can be referenced to recovery spallation and buckling.

Table 3 Critical load of coating failure modes determined with the scratch-test method for no sterilized and sterilized coated glass containers.

	Critical load (N)			
	Buckling-spallation mode	First cracks mode	Lateral cracking mode	Chipping mode
As processed	-	12.2	16.8	25.5
Sterilized	11.9	22.2	24.1	27.5

Comparison of critical loads among samples from different studies is only allowed if the coating-substrate system, the film thickness, the scratch-test apparatus, the scratch parameters and the applied load are the same. In this case, the chipping mode occurs at relatively high load which should lead to a satisfactory adhesion of the thin film. On the other hand, for sterilized coated container, an additional mode occurs (buckling/recovery spallation) for a mean load of 11.9 N. This mode is usually related to interfacial failure. It could be explained by a softer coating on a hard substrate where the adhesion is weak. However, the other cracking failure modes related to hard coating appear at higher loads than those for as processed coated container. These results suggest that the upper part of the alumina film is damaged by the sterilization cycle, making it porous, rough and soft. A lower part could remain non affected forming a hard, dense and adhesive layer on the glass surface.

4 Conclusions Alumina films were deposited by DLI-MOCVD from ATI at 5 Torr. Direct liquid injection technology generally allows a better control of generated reactive gaseous mass flow and vaporization, thereby contributing to a more robust process. Cyclohexane has been selected to dissolve and transport ATI to the deposition area. A very low amount of carbon (below 1 at%) is found in the film composition which proves the solvent does not readily decompose during deposition.

Films are amorphous in the temperature range 360-560 °C. Coatings processed at high temperatures (490-560 °C) correspond to stoichiometric Al_2O_3 with a very low amount of hydroxyl groups; the composition of those deposited at lower temperatures (360-420 °C) ranges from AlOOH to partially hydroxylated alumina $AlO_{1+x}(OH)_{1-2x}$ with increasing temperature. The film morphology is relatively smooth (RMS 17.1 nm) and slightly porous with nanometer cavities.

Amorphous alumina films were deposited on the inner surface of glass containers and heat treated in humid atmosphere. SEM observation and AFM imaging show that the sterilization cycle affects the surface topography and morphology, making the film rougher (RMS 61.7 nm) and more porous. It also affects the film adhesion on the glass surface as revealed by scratch-tests.

Supporting Information

Additional supporting information may be found in the online version of this article at the publisher's website.

Acknowledgements We are indebted to Djar Oquab, Yannick Thebault, Cedric Charvillat and Jérôme Esvan, from CIRIMAT for help with SEM, AFM XRD and XPS measurements respectively, to Philippe de Parseval, UMS Castaing, for the EPMA characterization, and to Florent Colomes and Iulian Stan for experimental study of ATI solubility. We also thank Hervé Guillon, Kemstream, Montpellier for advice on the operation of the DLI facility.

References

[1] D. H. Kuo, B. Y. Cheung, and R. J. Wu, Thin Solid Films **398**, 35-40 (2001).
[2] M. Voigt and M. Sokolowski, Mater. Sci. Eng. B **109**, 99-103 (2004).
[3] R. M'Saoubi and S. Ruppi, CIRP Ann-Manuf. Technol. **58**, 57-60 (2009).
[4] K. Haas-Santo, M. Fichtner, and K. Schubert, Appl. Catal. A **220**, 79-92 (2001).
[5] J. Masalski, J. Gluszek, J. Zabrzeski, K. Nitsch, and P. Gluszek, Thin Solid Films **349**, 186-190 (1999).
[6] C. F. Struller, P. J. Kelly, N. J. Copeland, and C. M. Liauw, J. Vac. Sci. Technol. A **30**, 041502-1-041502-8 (2012).
[7] D. Samelor, A. M. Lazar, M. Aufray, C. Tendero, L. Lacroix, J. D. Beguin, B. Caussat, H. Vergnes, J. Alexis, D. Poquillon, N. Pebere, A. Gleizes, and C. Vahlas, J. Nanosci. Nanotechnol. **11**, 8387-8391 (2011).
[8] D. Samélor, M. Aufray, L. Lacroix, Y. Balcaen, J. Alexis, H. Vergnes, D. Poquillon, J. D. Beguin, N. Pébère, S. Marcelin, B. Caussat, and C. Vahlas, Adv. Sci. Technol. **66**, 66-73 (2010).
[9] L. Wu, L. Song, J. Wu, L. Zhao, and C. Jiang, Ceram. Int. **747**, 747-750 (2007).
[10] M. D. Groner, F. H. Fabreguette, J. W. Elam, and S. M. George, Chem. Mater. **16**, 639-645 (2004).
[11] M. K. Tripp, C. Stampfer, D. C. Miller, T. Helbling, C. F. Hermann, C. Hierold, K. Gall, S. M. George, and V. M. Bright, Sens. Actuators A **130**, 419-429 (2006).
[12] S. Blittersdorf, N. Bahlawane, K. Kohse-Hoinghaus, B. Atakan, and J. Muller, Chem. Vap. Depos. **9**, 194-198 (2003).
[13] M. M. Sovar, D. Samélor, A. N. Gleizes, and C. Vahlas, Surf. Coat. Technol. **201**, 9159-9162 (2007).

[14] S. Krumdieck, S. Davies, C. M. Bishop, T. Kemmitt, and J. V. Kennedy, Surf. Coat. Technol. **230**, 208-212 (2013).
[15] A. N. Gleizes, C. Vahlas, M. M. Sovar, D. Samelor, and M. C. Lafont, Chem. Vap. Depos. **13**, 23-29 (2007).
[16] A. N. Gleizes, M.-M. Sovar, D. Samélor, and C. Vahlas, Adv. Sci. Technol. **45**, 1184-1193 (2006).
[17] H. Vergnes, D. Samelor, A. N. Gleizes, C. Vahlas, and B. Caussat, Chem. Vap. Depos. **17**, 181-185 (2011).
[18] R. W. J. Morssinkhof, The deposition of thin alumina films on steels by MOCVD. Synthesis, characterization and protective properties against high temperature corrosion (University of Twente, 1991).
[19] S. K. Soni, D. Samelor, B. W. Sheldon, C. Vahlas, and A. N. Gleizes, ECS Trans. **25**, 1309-1315 (2009).
[20] N. Y. Turova, V. A. Kozunov, A. I. Yanovskii, N. G. Bokii, Y. T. Struchkov, and B. L. Tarnopolskii, J. Inorg. Nucl. Chem. **41**, 5-11 (1979).
[21] M. Manin, S. Thollon, F. Emieux, G. Berthome, M. Pons, and H. Guillon, Surf. Coat. Technol. **200**, 1424-1429 (2005)
[22] J. Mungkalasiri, L. Bedel, F. Emieux, J. Dore, F. N. R. Renaud, and F. Maury, Surf. Coat. Technol. **204**, 887-892 (2009).
[23] M. K. Song, S. W. Kang, and S. W. Rhee, J. Electrochem. Soc. **152**, C108-C112 (2005).
[24] P. L. Etchepare, H. Vergnes, D. Samélor, D. Sadowski, C. Brasme, B. Caussat, and C. Vahlas, Adv. Sci. Technol. **91**, 117-122 (2014).
[25] P. L. Etchepare, H. Vergnes, D. Samélor, D. Sadowski, B. Caussat, and C. Vahlas, Surf. Coat. Technol. (2015, Submitted)
[26] A. Douard and F. Maury, Surf. Coat. Technol. **200**, 6267-6271 (2006).
[27] A. Hess, E. Kemnitz, A. Lippitz, W. E. S. Unger, and D.-H. Menz, J. Catalysis **148**, 270 (1994).
[28] H. He, K. Alberti, T. L. Barr, and J. Klinowski, J. Phys. Chem. **97,** 13703 (1993).
[29] J. T. Kloprogge, L. V. Duong, B. J. Wood, and R. L. Frost, J. Colloid Interf. Sci. **296**, 572 (2006).
[30] L. Baggetto, N. J. Dudney, and G. M. Veith, Electrochim. Acta **90**, 135 (2013).
[31] S. Verdier, L. El Ouatani, R. Dedryvère, F. Bonhomme, P. Biensan, and D. Gonbeau, J. Electrochem. Soc. **154**, A1088 (2007).
[32] Y. Balcaen, N. Radutoiu, J. Alexis, J. D. Beguin, L. Lacroix, D. Samelor, and C. Vahlas, Surf. Coat. Technol. **206**, 1684-1690 (2011).
[33] S. J. Bull, Surf. Coat. Technol. **50**, 25-32 (1991).
[34] C. H. Lin, H. L. Wang, and M. H. Hon, Thin Solid Films **283**, 171-174 (1996).